I R A M P
3(2), Dec. 2012, pp. 75-84

ISSN: 2229-3159

Generalized Collisional-Radiative Coefficients for Lithium in Debye-Huckel Plasmas

S. D. LOCH AND M. S. PINDZOLA

Department of Physics, Auburn University, Auburn, AL 36849

ABSTRACT: Generalized collisional-radiative (GCR) ionization and recombination coefficients are calculated for neutral Li using unscreened and screened atomic collision data in an n = 3 model. For electron densities up to 10^{14} cm^{-3}, no change is found in the GCR ionization and recombination coefficients whether using unscreened or screened atomic data. By 10^{18} cm^{-3}, reductions of 35% are seen at temperatures of 2 eV for the GCR ionization and recombination rate coefficients using the screened atomic data. Since the reductions are similar, the effect of using screened atomic data has little effect on Li/Li^{+} ionization balance calculations and photon emissivities. Continuum lowering for these conditions produces an increase in the ionization rate coefficients that is similar in size to the reduction caused by plasma screening effects. While there is an effect on the plasma equilibrium timescales, at the densities required for the plasma screening to become important it is unlikely that any measurable difference would be observed in the plasma.

1. INTRODUCTION

For many years generalized collisional-radiative theory has provided a means to process large atomic collision datasets into temperature and density dependent ionization and recombination rate coefficients that have proved very useful in gaining a better understanding of moderately dense astrophysical and magnetic fusion plasmas[1]. For example, the density effects on the ionization rates arise via processes such as collisional excitation to excited states followed by collisional ionization from excited states. On the other hand, for the very dense plasmas found in x-ray lasers and inertial confinement fusion plasmas, the basic atomic collision datasets are modified using various electron scattering screening methods [2].

While existing archives of generalized collisional-radiative coefficients include density effects through the excited states, no previous studies have investigated the density at which plasma screening corrections to the cross sections would change the generalized collisional-radiative coefficients. One key question is whether such effects should be considered in impurity transport modeling of magnetically confined fusion experiments.

In this article, we explore the effect of using a screening method on the basic electron-impact excitation and ionization cross sections to see at what densities the generalized collisional-radiative ionization and recombination rate coefficients begin to be affected. Recent work using screened potentials in an R-matrix with pseudostates calculation for electron-impact excitation of the H atom [3] and in a converged close-coupling calculation for electron-impact excitation and ionization of the He atom [4], have provided an incentive for us to look at the use of screened potentials in distorted-wave calculations for the electron-impact excitation and ionization of the Li atom. Before modifying our own R-matrix and close-coupling codes to include screened potentials, we first wanted to use previous screened distorted-wave codes [5] to explore the densities at which the screening effects become important. Using the screened atomic collision dataset, we then carried out generalized collisional-radiative calculations for temperature and density dependent ionization and recombination rate coefficients. We first explored the validity of our model, comparing it with previous GCR datasets. The screened generalized collisional-radiative derived atomic dataset then allowed us to investigate the effects on ionization balance, emissivity, ionizations per photon, and equilibrium timescales for a low temperature Li plasma.

The remainder of this article is organized as follows: in Section II we provide an overview of theoretical methods, in Section III we present our cross section results, discuss the validity of our model and present the generalized collisional-radiative results. In Section IV we conclude with a brief summary. Unless otherwise stated, all quantities are given in atomic units.

2. THEORY

2.1. Debye-Huckel Screened Cross Sections

For electron-impact excitation, a general transition between configurations has the form:

$$\left(n_1 l_1\right)^{\omega_1}\left(n_2 l_2\right)^{\omega_2} k_i l_i \rightarrow \left(n_1 l_1\right)^{\omega_1 - 1}\left(n_2 l_2\right)^{\omega_2 + 1} k_f l_f \tag{1}$$

where ω_i are subshell occupation numbers, $n_i l_i$ are quantum numbers of the bound electrons, and $k_i l_i$, $k_f\, l_f$ are quantum numbers of the initial and final continuum electrons. The configuration-average cross section is given by [6]:

$$\sigma_{exc} = \frac{8\pi}{k_i^3 k_f}\left(4l_2 + 2 - \omega_2\right)\sum_{l_i, l_f}\left(2l_i + 1\right)\left(2l_f + 1\right) S\left(n_1 l_1 k_i l_i \rightarrow n_2 l_2 k_f l_f\right). \tag{2}$$

For electron-impact ionization, a general transition between configurations has the form:

$$\left(nl\right)^{\omega} k_i l_i \rightarrow \left(nl\right)^{\omega_1 - 1} k_e l_e k_f l_f\,, \tag{3}$$

where $k_i l_i$, $k_e l_e$, $k_f l_f$ are quantum numbers of the initial, ejected, and final continuum electrons. The configuration-average cross section is given by [6]:

$$\sigma_{exc} = \frac{32\omega}{k_i^3}\int_0^{E/2}\frac{d\left(k_e^2/2\right)}{k_e k_f}\sum_{l_i, l_e, l_f}\left(2l_i + 1\right)\left(2l_e + 1\right)\left(2l_f + 1\right) S\left(nlk_i l_i \rightarrow k_e l_e k_f l_f\right). \tag{4}$$

where $E = (k_e^2 + k_f^2)/2$. The scattering matrices, $S(n_1 l_1\, k_i l_i \rightarrow n_2 l_2\, k_f l_f)$ and $S(nl\, k_i l_i \rightarrow k_e l_e\, k_f l_f)$, are sums over products of standard angular factors and radial direct and exchange electrostatic integrals.

The Debye-Huckel screening radius is given by [7]:

$$\Lambda = \sqrt{\frac{T_e}{4\pi N_e}}\,, \tag{5}$$

where T_e is the electron temperature (1 a.u. = 27.212 eV) and N_e is the electron density (1 a.u. = 6.75 x 10^{24} cm^{-3}). The initial ($k_i\, l_i$) and final ($k_f l_f$) distorted-waves are found by solving a single-channel radial Schrodinger equation given by:

$$\left(-\frac{1}{2}\frac{d^2}{dr^2} + \frac{l(l+1)}{2r^2} - \frac{Z}{r}e^{-r/\Lambda} + V_{HX}^N(r)e^{-r/\Lambda} - \frac{k^2}{2}\right)P_{kl}(r) = 0, \tag{6}$$

where Z is the nuclear charge and $V_{HX}^N(r)$ is an N electron Hartree with local exchange potential. In keeping with a widely used moderately dense plasma approximation [8], no screening factors are used to modify the potential terms for the bound and ejected electrons. In addition, the direct electrostatic radial matrix elements found in the scattering matrices of Eqs.(2) and (4) are given by:

$$R^{\lambda}\left(n_1 l_1 k_i l_i \rightarrow n_2 l_2 k_f l_f\right) = \int_0^{\infty} dr_1 \int_0^{\infty} dr_2 \frac{r^{\lambda}}{r^{\lambda+1}} e^{-r_2/\Lambda} P_{n_1 l_1}(r_1) P_{k_i l_i}(r_2) P_{n_2 l_2}(r_1) P_{k_f l_f}(r_2), \tag{7}$$

$$R^{\lambda}\left(nlk_i l_i \rightarrow k_e l_e k_f l_f\right) = \int_0^{\infty} dr_1 \int_0^{\infty} dr_2 \frac{r^{\lambda}}{r^{\lambda+1}} e^{-r_2/\Lambda} P_{nl}(r_1) P_{k_i l_i}(r_2) P_{k_e l_e}(r_1) P_{k_f l_f}(r_2), \tag{8}$$

where $r = \min(r_1, r_2)$ and $r = \max(r_1, r_2)$.

2.2. Collisional-Radiative Modeling

The standard collisional-radiative equations to determine ground and excited state populations, N_j^z, for each ion stage z of an atom in a plasma are given by [9]:

$$\begin{aligned} \frac{dN_j^z}{dt} &= -\sum_{j'<j} A_{j\rightarrow j'} N_j^z - N_e \sum_{j'\neq j} q_{j\rightarrow j'} N_j^z + \sum_{j'>j} A_{j'\rightarrow j} N_{j'}^z \\ &+ N_e \sum_{j'\neq j} q_{j'\rightarrow j} N_{j'}^z - N_e \sum_k s_{j\rightarrow k} N_j^z + N_e \sum_k r_{k\rightarrow j} N_k^{z+1}, \end{aligned} \tag{9}$$

$A_{j\rightarrow j'}$ are radiative decay rates, $q_{j\rightarrow j'}$ are electron-impact excitation rates, $s_{j\rightarrow k}$ are electron-impact ionization rates, $r_{k\rightarrow j}$ are electron-impact recombination rates, and N_e is the electron density. The excitation, ionization, and recombination rates are all obtained by integrating the appropriate electron-atom cross sections over a Maxwellian electron temperature distribution.

For many plasma conditions, the ground and metastable state populations, N_β^z, evolve on a much slower timescale than the excited state populations, allowing the time derivative of the excited state populations to be set to zero. In the quasi-static equilibrium approximation, the ground and metastable state populations can be calculated via the generalized collisional-radiative (GCR) equations [10]:

$$\begin{aligned} \frac{dN_\beta^z}{dt} &= -N_e \sum_{\beta'\neq\beta} \left(X_{\beta\rightarrow\beta'} + Q_{\beta\rightarrow\beta'}\right) N_\beta^z + N_e \sum_{\beta'\neq\beta} \left(X_{\beta'\rightarrow\beta} + Q_{\beta'\rightarrow\beta}\right) N_{\beta'}^z \\ &- N_e \sum_\gamma S_{\beta\rightarrow\gamma} N_\beta^z + N_e \sum_\alpha S_{\alpha\rightarrow\beta} N_\alpha^{z-1} + N_e \sum_\gamma R_{\gamma\rightarrow\beta} N_\gamma^{z+1} - N_e \sum_\alpha R_{\beta\rightarrow\alpha} N_\alpha^z \end{aligned} . \tag{10}$$

The cross-coupling rate coefficients are given by:

$$X_{\beta\rightarrow\beta'} = \left(C_\beta^z - \sum_j C_{\beta' j}^z \sum_{j'} \left(C_{jj'}^z\right)^{-1} C_{j'\beta}^z \right) / N_e \tag{11}$$

and the parent cross-coupling rate coefficients are given by:

$$Q_{\beta\rightarrow\beta'} = N_e \sum_i s_{i\rightarrow\beta'} \sum_{i'} \left(C_{ii'}^{z-1}\right)^{-1} r_{\beta\rightarrow i'}, \tag{12}$$

where the collisional-radiative matrix elements for ion stage z are given by:

$$C_{jj}^z = \sum_{j'<j} A_{j\rightarrow j'} + N_e \sum_{j'\neq j} q_{j\rightarrow j'}, \tag{13}$$

$$C_{jj'}^z = -A_{j'\rightarrow j} - N_e q_{j'\rightarrow j} \qquad \text{for j}' > \text{j} \tag{14}$$

$$C_{jj'}^z = -N_e q_{j'\rightarrow j} \qquad \text{for j}' < \text{j} \tag{15}$$

The generalized ionization rate coefficients are given by:

$$S_{\beta\to\gamma} = s_{\beta\to\gamma} - \sum_j s_{j\to\gamma} \sum_{j'} \left(C^z_{jj'}\right)^{-1} C^z_{j'\beta}, \tag{16}$$

$$S_{\alpha\to\beta} = s_{\alpha\to\beta} - \sum_i s_{i\to\beta} \sum_{i'} \left(C^{z-1}_{ii'}\right)^{-1} C^{z.}_{i'\alpha} . \tag{17}$$

The generalized recombination rate coefficients are given by:

$$R_{\gamma\to\beta} = r_{\gamma\to\beta} - \sum_j C^z_{\beta j} \sum_{j'} \left(C^z_{jj'}\right)^{-1} r_{\gamma\to j'}, \tag{18}$$

$$R_{\beta\to\alpha} = r_{\beta\to\alpha} - \sum_i C^{z-1}_{\alpha i} \sum_{i'} \left(C^{z-1}_{ii'}\right)^{-1} r_{\beta\to i'}. \tag{19}$$

These generalized collisional-radiative coefficients are a function of both temperature and density. In the case of no metastables, or the "stage to stage" model, there are no cross-coupling rate coefficients, $X_{\beta\to\beta}$ and $Q_{\beta\to\beta}$. We note that it is these generalized collisional-radiative coefficients that are most useful in plasma impurity transport codes, since they contain the effects of the excited states on the ground and metastables, without the need for a large number of coefficients to be archived.

3. RESULTS

In this section we first describe the atomic data in our model, showing the effects of screening on the cross sections. We note that these are the first published calculations including screening for neutral Li. We then discuss the validity of our n = 3 collisional-radiative model, comparing it with previous Li GCR datasets. The GCR coefficients produced using our new data are described, and the effects of plasma screening on the GCR coefficients are discussed. Finally, we discuss the implications of this work on plasma ionization balance, spectral emission and equilibrium timescales.

3.1. Atomic Collision Data Sets

Excitation, ionization, and recombination rate coefficients for neutral Li were generated as follows. In all cases, only the $1s^2 2l$ and $1s^2 3l$ configurations were considered. The spontaneous emission rates were taken from R-matrix calculations [11], the same A-values that were used in the recommended GCR data for Li [12].

The electron-impact excitation cross sections and rate coefficients were calculated from configuration-average distorted-wave calculations using Eq. (2). All transitions among the 2s, 2p, 3s, 3p, 3d subshells were generated. Cross sections with and without plasma screening effects were calculated. The screened cross sections were evaluated for Debye-Huckel screening radii corresponding to T_e = 0.35 eV with $N_e = 10^{14}$ cm^{-3} and $N_e = 10^{18}$ cm^{-3}. The temperature chosen lies in the range where neutral Li and Li^+ abundances are similar for moderately dense plasmas ($N_e = 10^{14}$ cm^{-3}).

The electron-impact ionization cross sections and rate coefficients were calculated from configuration-average distorted-wave calculations using Eq. (4). All transitions from the 2s, 2p, 3s, 3p, 3d subshells were generated. Again, cross sections with and without plasma screening effects were calculated. The screened cross sections were again evaluated for Debye-Huckel screening radii corresponding to T_e= 0.35 eV, with $N_e = 10^{14}$ cm^{-3}, $N_e = 10^{16}$ cm^{-3}, $N_e = 10^{18}$ cm^{-3}, and $N_e = 10^{20}$ cm^{-3}. Unscreened and screened ionization cross sections at 2.0 times the ionization potential are given in Table I. At $N_e = 10^{18}$ cm^{-3} there is an 11% reduction in the 2s cross section, a 14% reduction in the 2p cross section, a 25% reduction in the 3s cross section, a 29% reduction in the 3p cross section, and a 27% reduction in the 3d cross section.

Unscreened and $N_e = 10^{18}$ cm^{-3} screened ionization cross sections over a wide energy range are shown in Figure 1 for the 2s and 2p subshells and in Figure 2 for the 3s, 3p, and 3d subshells. In the generalized collisional-radiative

modeling we are primarily interested in the effects of screening at temperatures close to that chosen in the Debye-Huckel screening. This Maxwellian temperature is below the ionization potentials for all the subshells. Thus, the important part of each cross section is the near threshold section. For example, at $N_e = 10^{18}$ cm^{-3} and 1.1 times the ionization potential there is a 16% reduction in the 2s cross section, a 36% reduction in the 2p cross section, a 23% reduction in the 3s cross section, a 56% reduction in the 3p cross section, and a 30% reduction in the 3d cross section.

The radiative recombination (RR) rate coefficients were generated using a Gaunt factor approach [13]. No screening was included in the radiative recombination calculations due to the small effect that this process has on the modeling at these densities. Screened and unscreened dielectronic recombination (DR) rate coefficients were generated using the AUTOSTRUCTURE code [14], using an *n*-cutoff given by:

$$n = \left(\frac{3}{4\pi N_e} \right)^{1/6} . \tag{20}$$

As will be shown later in this section, dielectronic recombination is not the dominant recombination mechanism for the plasma conditions where the plasma screening effects start to become important. Thus, we have three atomic collision datafiles for use in our collisional-radiative modeling. File 1 contains radiative, excitation, ionization, and recombination rate coefficients based upon completely unscreened cross sections. File 2 contains rate coefficients which include the effects of plasma screening on the collision data appropriate for T_e = 0.35 eV and $N_e = 10^{14}$ cm^{-3} conditions. File 3 contains rate coefficients which include the effects of plasma screening on the collision data appropriate for T_e= 0.35 eV and $N_e = 10^{18}$ cm^{-3} conditions. Note that for File 2 and File 3, the rate coefficients should still be reasonably accurate for temperatures close to 0.35 eV, due to the $T_e^{1/2}$ dependence of the Debye-Huckel screening radius. Thus, we will show results that cover a temperature range from 0.10 eV through to 7.0 eV.

3.2. Validity of the Current Model

Before describing our generalized collisional radiative results and the implications of plasma screening, we first consider the validity of our model. We have compared our n = 3 generalized collisional-radiative ionization rate coefficient produced using Eq. (16) with those from a dataset involving higher n-shells [12]. At the lower temperatures (<5eV), the differences are about 30%, with our results being lower than the data from [12]. Thus, our results are not as different from a higher-n model as one might expect, as long as we restrict ourselves to these lower temperatures. The reasons for the relatively small difference is that at these higher densities the populations are driven to their Local Thermodynamic Equilibrium values. However, the absolute value for the excited populations is small due to the low value of T_e in the Saha-Boltzman equation. Thus, the contribution to the effective ionization due to the high-n populations falls off quite quickly with n-shell. Also, the DW ionization cross sections for n=2 and 3 are not hugely different from the non-perturbative data used in Loch *et al.* [12]. So the GCR ionization rate coefficient from our n=3 model is close to that from previous studies. The discrepancy becomes larger if on goes beyond 5eV.

We also considered the role of continuum lowering on the ionization rate coefficients for N_e = 1 x 10^{18} cm^{-3}. While continuum lowering was not included in our distorted-wave ionization calculations, we can include it when generating the ionization rate coefficients. Using the screened cross sections shown in Figs. 1 and 2, we introduced a continuum lowering of 0.12 eV, corresponding to a Debye ionization potential lowering for N_e = 1x10^{18} cm^{-3}. This results in an increase in the ionization rate coefficients of about 10-30% for the subshells within the n = 3 shell. In turn the GCR ionization rate coefficient increases by about 30%. We note that the same percentage change is seen in our 3-body recombination rate coefficients, since they are produced from detailed balance using the ionization rate coefficients. At the higher densities considered in this study, the ionization balance is dominated by collisional ionization and 3-body recombination.

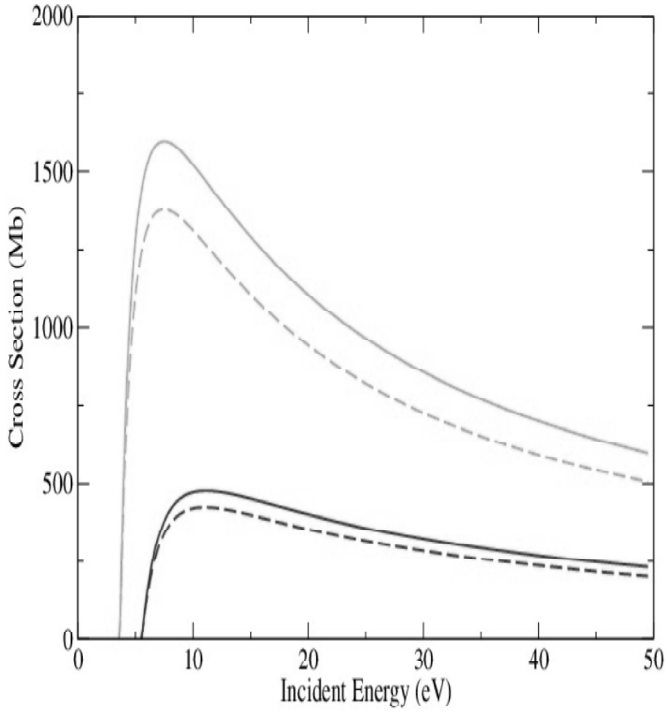

Figure 1: Direct ionization cross sections for Li($1s^2$ 2*l*). Lowest solid (red) curve: 2s subshell with no screening, lowest dashed (red) curve: 2s subshell with $N_e = 10^{18}$ cm^{-3}, highest solid (green) curve: 2p subshell with no screening, highest dashed (green) curve: 2p subshell with $N_e = 10^{18}$ cm^{-3} (1.0 Mb = 1.0 x 10^{-18} cm^2)

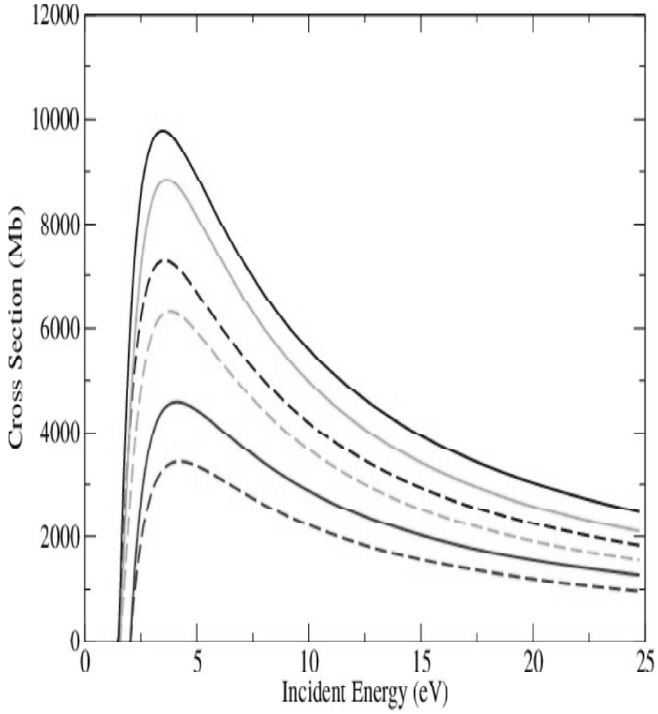

Figure 2: Direct ionization cross sections for Li($1s^2$ 3*l*). Lowest solid (red) curve: 3s subshell with no screening, lowest dashed (red) curve: 3s subshell with $N_e = 10^{18}$ cm^{-3}, middle solid (green) curve: 3p subshell with no screening, middle dashed (green) curve: 3p subshell with $N_e = 10^{18}$ cm^{-3}, highest solid (blue) curve: 3d subshell with no screening, highest dashed (blue) curve: 3d subshell with $N_e = 10^{18}$ cm^{-3} (1.0 Mb = 1.0 x 10^{-18} cm^2)

We would point out that we are not attempting to produce the definitive dataset for high density Li studies, but to determine the density at which screening effects on the cross section have to be included in GCR calculations, for which this model should be sufficient.

3.3. Generalized Collisional-Radiative Modeling

Generalized collisional-radiative ionization rate coefficients calculated using Eq. (16) are shown in Figure 3. The GCR results with unscreened cross sections are shown for $N_e = 10^{14}$ cm^{-3} and 10^{18} cm^{-3}, along with their corresponding screened results. Also shown are ground state ionization rate coefficients. The importance of the excited states in ionization can be seen from the large increase in the ionization rate coefficients compared with the ground state rate coefficients. Despite using distorted-wave cross sections, instead of non-perturbative calculations [11, 15], our results show a similar increase to that generated from the non-perturbative dataset of Loch *et al.* [12]. The unscreened results for $N_e = 10^{18}$ cm^{-3} are very close to the unscreened results for $N_e = 10^{14}$ cm^{-3}. This is due to the fact that the excited populations are close to their (LTE) values, and so no longer depend upon the electron-impact excitation cross sections and rate coefficients.

The differences due to the effects of plasma screening can also be seen in Figure 3. At $N_e = 10^{14}$ cm^{-3} the screened results are extremely close to the unscreened results, as one might expect from the small change in the underlying cross sections. At $N_e = 10^{18}$ cm^{-3} there is a 35% reduction in the GCR ionization rate coefficient at $T_e = 2.0$ eV, similar in size to the reduction in the underlying cross sections. If continuum lowering is also included, then the ionization rate coefficients return to close to their unscreened values.

Generalized collisional-radiative recombination rate coefficients calculated using Eq. (18) are shown in Figure 4. The unscreened results in the low density limit with excited states are significantly higher than the low

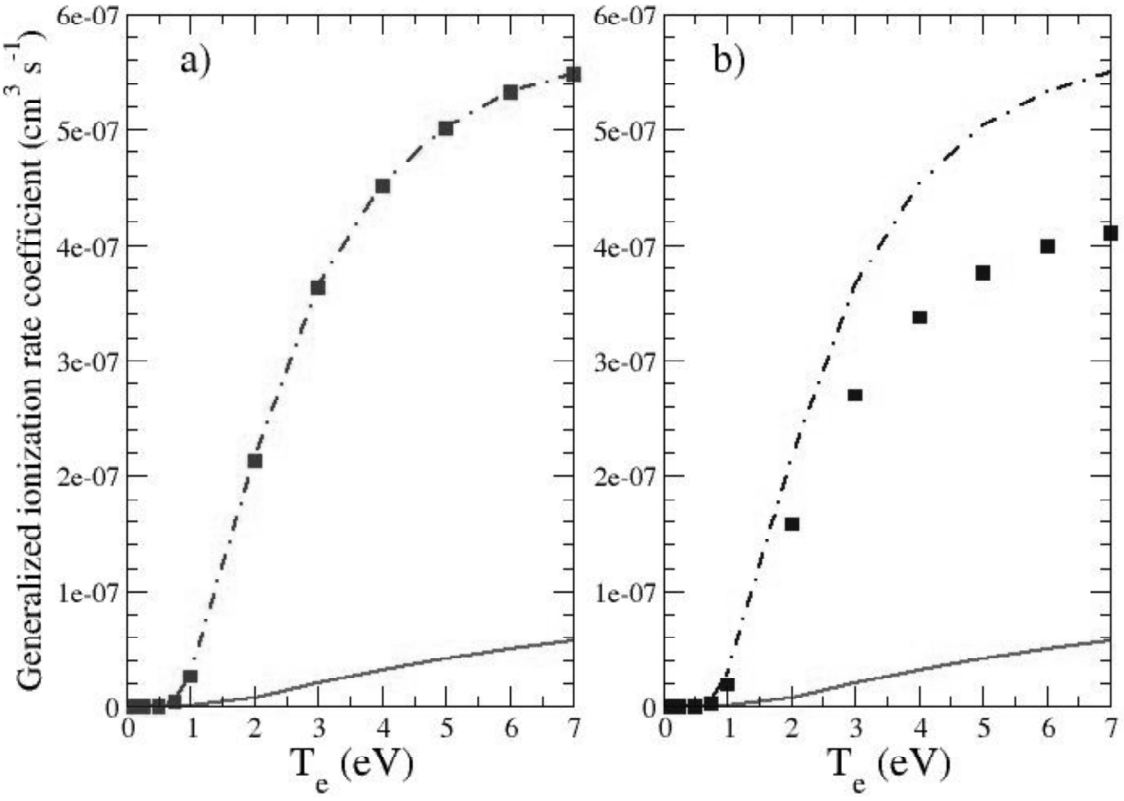

Figure 3: GCR ionization rate coefficient for Li. (a) solid (green) line: low density limit with no screening, dot-dash (red) line: $N_e = 10^{14}$ cm^{-3} with no screening, solid (red) squares: $N_e = 10^{14}$ cm^{-3} with screening, (b) solid (green) line: low density limit with no screening, dot-dash (blue) line: $N_e = 10^{18}$ cm^{-3} with no screening, solid (blue) squares: $N_e = 10^{18}$ cm^{-3} with screening

density limit without excited states (i.e. only $1s^2 \rightarrow 1s^2\ 2s$) recombination rate coefficient. This reflects the fact that even at low densities, the excited states are an important route for recombination (followed by radiative cascades to the ground). At $N_e = 10^{14}$ cm^{-3} the unscreened and screened results are essentially the same. For $N_e = 10^{18}$ cm^{-3}, 3-body recombination dominates over DR and RR as the main recombination process. The three-body recombination rate coefficients are evaluated from the ionization rate coefficient via the well known detailed balance relationship. Thus, the 35% reduction in the GCR recombination rate coefficient at $T_e = 2.0$ eV is due primarily to the reduction in the ionization cross section. Similarly, when continuum lowering is included in the ionization cross sections, there is subsequent increase in the recombination rate coefficient by about 30%.

3.4. Ionization Balance, Emissivity, Ionizations per Photon, and Equilibrium Timescales

If one uses the GCR ionization and recombination rate coefficients to evaluate an equilibrium ionization balance (i.e. Eq.(10) with the dN/dt values set to zero), then one finds that in both the screened and unscreened cases, the temperature at which Li^+ starts to exist gradually increases as the density increases. This is due to the relative increase in the recombination rate compared with ionization. Three-body recombination scales as N_e^2, which in turn makes recombination dominate over ionization up to higher temperatures. However, since the effects of plasma screening on the GCR ionization and recombination rate coefficients are to reduce them by the same fraction, the ionization balance produced using the screened atomic data is the same as in the unscreened case.

The effects of plasma screening on the photon emission are also negligible at $N_e = 10^{18}$ cm^{-3}. At the lower densities, before the excited populations reach their LTE values, the effects of screening on the excitation cross sections are small. For the densities at which the plasma screening effects start to become important, the populations are already at their LTE values, so are not altered by the screened cross sections.

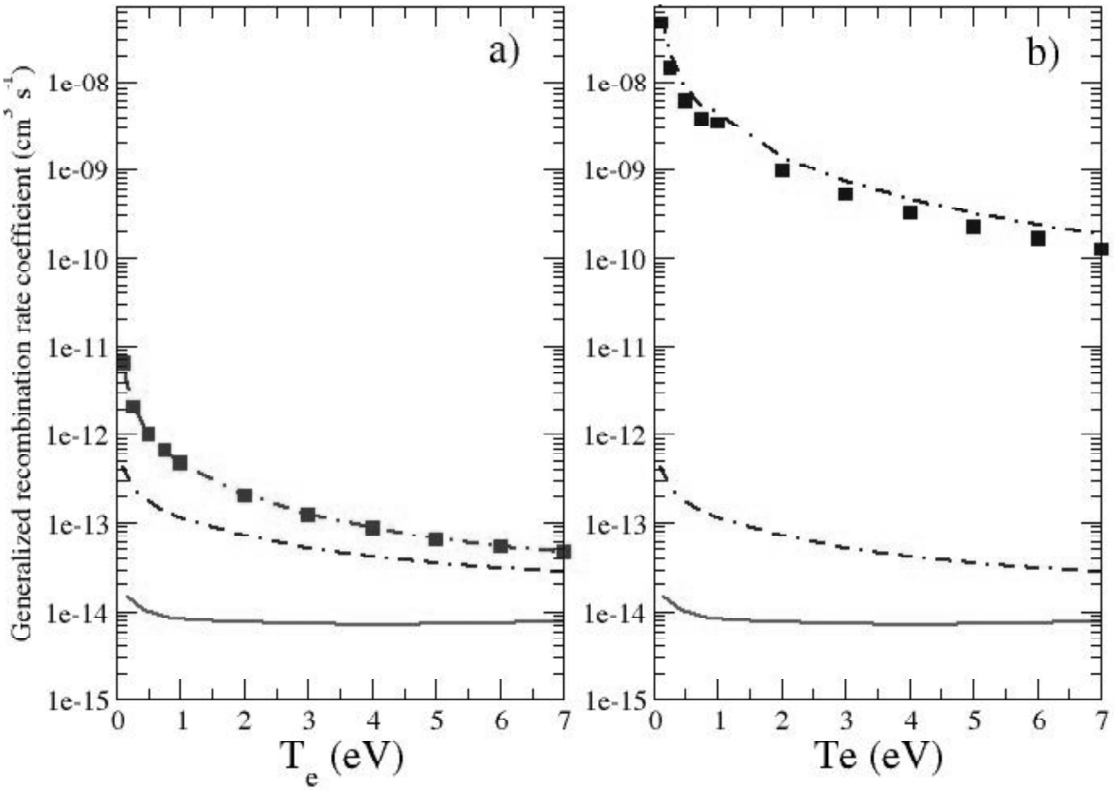

Figure 4. GCR recombination rate coefficient for Li. (a) solid (green) line: low density limit, with no excited states, with no screening, dot-double dash (purple) line: low density limit, with excited states, with no screening, dot-dash (red) line: $N_e = 10^{14}$ cm^{-3}, with excited states, with no screening, solid (red) squares: $N_e = 10^{14}$ cm^{-3}, with excited states, with screening, (b) solid (green) line: low density limit, with no excited states, with no screening, dot-double dash (purple) line: low density limit, with excited states, with no screening, dot-dash (blue) line: $N_e = 10^{18}$ cm^{-3}, with excited states, with no screening, solid (blue) squares: $N_e = 10^{18}$ cm^{-3}, with excited states, with screening

The screening effects on ionizations per photon (SXB) coefficients, a commonly used diagnostic for impurity influx, are more marked. The SXB coefficient is the ratio of the GCR ionization rate coefficient divided by a particular photon emissivity coefficient and can be directly related to the impurity influx from a vessel wall. The SXB will be altered by exactly the same amount as the GCR ionization rate coefficient, namely 35% at $N_e = 10^{18}$ cm^{-3}, due to the fact that the GCR ionization rate has been reduced while the photon emissivity is unchanged with increasing density. However, once continuum lowering is included in the ionization rate coefficients the difference with the unscreened SXB results would be small.

The other plasma parameter that would be altered by the plasma screening effect is the ionization equilibrium timescale. If we restrict ourselves to temperatures at which only Li and Li^+ can exist, then the time constant for the Li to reach its equilibrium ionization value is given by the reciprocal of the sum of the ionization and recombination rate coefficients times the electron density. Thus, a 35% reduction on both rates will produce a marked difference in the time for the plasma to reach equilibrium. Of course, for dense plasmas such as these, the plasma reaches equilibrium in a very short timescale, so the effect may not be measurable. For example, at $N_e = 10^{18}$ cm^{-3} and $T_e = 0.35$ eV the unscreened atomic data give an equilibrium time constant of 7.4×10^{-11} sec, while the screened atomic data give an equilibrium time constant of approximately 1.0×10^{-10} sec. The results with screening and continuum lowering would be close to the unscreened results.

4. SUMMARY

The effects of plasma screening on collision cross sections have been presented for neutral lithium. The effects on generalized collisional-radiative ionization and recombination rate coefficients have also been shown. At densities

Table 1
Electron-impact ionization cross sections at 2.0 times the ionization potential for Li($1s^2$ *nl*) all units are in Mb (1.0 Mb = 1.0 x 10^{-18} cm^2)

Subshell Density	*Unscreened*	*Screened 10^{14} cm^{-3}*	*Screened 10^{16} cm^{-3}*	*Screened 10^{18} cm^{-3}*	*Screened 10^{20} cm^{-3}*
2s	478	477	472	425	164
2p	1617	1615	1593	1396	433
3s	4516	4503	4386	3389	462
3p	8596	8566	8293	6082	653
3d	9627	9597	9331	7065	1027

important for magnetically confined tokamak edge plasmas, up to 10^{14} cm^{-3}, the effects of plasma screening on the cross sections are negligible and conventional generalized collisional-radiative coefficients are perfectly adequate for plasma modeling. At densities of 10^{18} cm^{-3}, the most important plasma screening effects to include are on the ionization cross sections. Dielectronic recombination is negligible compared with 3-body recombination, and changes to the excitation cross sections do not affect the populations, which are at their LTE values. At densities of 10^{18} cm^{-3}, there are 10% to 50% reductions in the ionization cross sections, which are seen as a 35% reduction in the generalized collisional-radiative ionization rate coefficient at T_e = 2.0 eV. Continuum lowering results in an increase of the ionization rate coefficients, returning the effective ionization rate coefficient to values close to the unscreened data. At this density three-body recombination dominates the GCR recombination coefficient, so we also see a 35% reduction in this coefficient when plasma screening is included. Continuum lowering results in an increase in the three-body recombination rate coefficients by close to the same amount. The photon emissivities are unchanged by plasma screening due to the excited populations being driven to their local thermodynamic equilibrium values. The changes to the GCR ionization and recombination rate coefficients cancel when the equilibrium fractional abundances are calculated due to both coefficients being reduced by the same amount. Thus, it does not appear that plasma screening effects are likely to be important for plasma modeling with light neutral species. The densities required for the screening effects to become important result in plasma conditions that minimize any observable different on the plasma. If one were to consider more complex neutral species, such as tungsten, the situation might be quite different. The density would be much lower for the plasma screening effects to become significant, the populations may not be in LTE at that point, and the recombination may not be dominated solely by three-body recombination. Due to the importance of tungsten for the fusion tokamak plasma experiments, this would be a useful area of future study.

Acknowledgments

This work was supported in part by grants from the US Department of Energy and the IAEA Nuclear Data Section to Auburn University. Computational work was carried out at the National Energy Research Scientific Computing Center in Oakland, California.

References

[1] H. P. Summers, W. J. Dickson, M. G. O'Mullane, N. R. Badnell, A. D. Whiteford, D. H. Brooks, J. Lang, S. D. Loch, and D. C. Griffin, *Plasma Phys. Control. Fusion* **48**, 263, (2006).

[2] M. S. Murillo and J. C. Weisheit, *Phys. Rep.* **302**, 1, (1998).

[3] S. B. Zhang, J. G. Wang, and R. K. Janev, *Phys. Rev. Letts.* **104**, 023203, (2010).

[4] M. C. Zammit, D. V. Fursa, I. Bray, and R. K. Janev, *Phys. Rev. A* **84**, 052705, (2011).

[5] M. S. Pindzola, S. D. Loch, J. Colgan, and C. J. Fontes, *Phys. Rev. A* **77**, 062707, (2008).

[6] M. S. Pindzola, D. C. Griffin, and C. Bottcher, NATO Advanced Studies Institute B **145**, 75, (1986).

[7] P. Debye and E. Hückel, Z. *Phys.* **24**, 185, (1923).

[8] B. L. Whitten, N. F. Lane, and J. C. Weisheit, *Phys. Rev. A* **29**, 945, (1984).

[9] D. R. Bates, A. E. Kingston, and R. W. P. McWhirter, Proc. Roy. Soc. London **267**, 297, (1962).

[10] R. W. P. McWhirter and H. P. Summers, *Applied Atomic Collision Physics* **2**, 51, (1984).

[11] D. C. Griffin, D. M. Mitnik, J. Colgan, and M. S. Pindzola, *Phys. Rev. A* **64**, 032718, (2001).

[12] S. D. Loch, J. Colgan, M. C. Witthoeft, M. S. Pindzola, C. P. Ballance, D. M. Mitnik, D. C. Griffin, M. G. O'Mullane, N. R. Badnell, and H. P. Summers, Atomic Data and Nuclear Data Tables **92**, 813, (2006).

[13] A. Burgess and H. P. Summers, Mon. Not. Roy. *Astron. Soc.* **174**, 345, (1976).

[14] N. R. Badnell, *J. Phys. B* **39**, 4825, (2006).

[15] J. Colgan, M. S. Pindzola, D. M. Mitnik, D. C. Griffin, and I. Bray, *Phys. Rev. Letts.* **87**, 213201, (2001).